

# JAAS

Accepted Manuscript



This is an *Accepted Manuscript*, which has been through the Royal Society of Chemistry peer review process and has been accepted for publication.

*Accepted Manuscripts* are published online shortly after acceptance, before technical editing, formatting and proof reading. Using this free service, authors can make their results available to the community, in citable form, before we publish the edited article. We will replace this *Accepted Manuscript* with the edited and formatted *Advance Article* as soon as it is available.

You can find more information about *Accepted Manuscripts* in the [Information for Authors](#).

Please note that technical editing may introduce minor changes to the text and/or graphics, which may alter content. The journal's standard [Terms & Conditions](#) and the [Ethical guidelines](#) still apply. In no event shall the Royal Society of Chemistry be held responsible for any errors or omissions in this *Accepted Manuscript* or any consequences arising from the use of any information it contains.

1  
2  
3  
4  
5 1  
6  
7 2  
8  
9  
10 3  
11  
12 4  
13  
14 5  
15  
16 6  
17  
18  
19 7  
20  
21 8  
22  
23 9  
24  
25 10  
26  
27 11  
28 12  
29 13  
30 14  
31 15  
32 16  
33 17  
34 18  
35 19  
36 20  
37 21  
38 22  
39 23  
40 24  
41 25  
42 26  
43 27  
44 28  
45 29  
46 30  
47 31  
48 32  
49 33  
50 34  
51 35  
52 36  
53 37  
54 38  
55 39  
56 40  
57 41  
58 42  
59 43  
60 44

## *Lead Isotope Analysis of Melt Inclusions by LA-MC-ICP-MS*

Le Zhang,<sup>a,b</sup> Zhong-Yuan Ren,<sup>\*a</sup> Alexander R. L. Nichols,<sup>c</sup> Yin-Hui Zhang,<sup>a,b</sup> Yan Zhang,<sup>a,b</sup>  
Sheng-Ping Qian<sup>a,b</sup> and Jian-Qiang Liu<sup>a,b</sup>

<sup>a</sup> *State Key Laboratory of Isotope Geochemistry, Guangzhou Institute of Geochemistry, Chinese Academy of Sciences, Guangzhou 510640, China*

<sup>b</sup> *University of Chinese Academy of Sciences, Beijing 100049, China*

<sup>c</sup> *Institute for Research on Earth Evolution (IFREE), Japan Agency for Marine Earth Science and Technology (JAMSTEC), 2-5 Natsushima-cho, Yokosuka, Kanagawa 237-0061, Japan*

\*Corresponding author:

Guangzhou Institute of Geochemistry

Chinese Academy of Sciences

510640 Wushan, Guangzhou

P. R. China

Tel: 86-20-85292969

Fax: : 86-20-85291510

E-mail: [zyren@gig.ac.cn](mailto:zyren@gig.ac.cn)

1  
2  
3  
4  
5  
6  
7  
8  
9  
10  
11  
12  
13  
14  
15  
16  
17  
18  
19  
20  
21  
22  
23  
24  
25  
26  
27  
28  
29  
30  
31  
32  
33  
34  
35  
36  
37  
38  
39  
40  
41  
42  
43  
44  
45  
46  
47  
48  
49  
50  
51  
52  
53  
54  
55  
56  
57  
58  
59  
60

**Abstract** Pb isotope compositions of melt inclusions provide unique information about the composition of primary magmas and their source. In this study, we have developed a method to measure Pb isotopes in small olivine-hosted melt inclusions (>40  $\mu\text{m}$ ) from young and old volcanoes by LA-MC-ICP-MS. We used a new interface cone assemblage consisting of a Jet sample cone and X skimmer cone. A small flow of  $\text{N}_2$  gas was added to the carrier gas and passed through the assemblage to enhance the signal intensity. In addition the energy and repetition rate of the laser condition were reduced and the signal integration time was shortened in order to lengthen the laser ablation time and to collect enough data. Mass bias and instrument drift were corrected using a standard-sample-standard bracketing method. The analysis routine employed eight ion counters to receive  $^{238}\text{U}$ ,  $^{235}\text{U}$ ,  $^{232}\text{Th}$ ,  $^{208}\text{Pb}$ ,  $^{207}\text{Pb}$ ,  $^{206}\text{Pb}$ ,  $^{204}\text{Pb}$  and  $^{202}\text{Hg}$  signals simultaneously, which allowed Hg interference to be corrected on  $^{204}\text{Pb}$ , and in old samples U-Th decay to be age-corrected. Using the Jet and X cones, under the same laser ablation conditions, the precisions for almost all the measured standard glasses are improved by at least a factor of two compared to using standard cones. At  $^{208}\text{Pb}$  signal intensity >200000 cps, external precisions of ratios involving  $^{204}\text{Pb}$  are better than 1.3% (2RSD) and precisions of  $^{208}\text{Pb}/^{206}\text{Pb}$  and  $^{207}\text{Pb}/^{206}\text{Pb}$  are better than 0.23% (2RSD). The results of Pb isotopes in olivine-hosted melt inclusions, using 45  $\mu\text{m}$  laser spots, show that the internal precisions of  $^{208}\text{Pb}/^{206}\text{Pb}$  and  $^{207}\text{Pb}/^{206}\text{Pb}$  for most analyzed melt inclusions are better than 0.2% (2RSE) and for ratios involving  $^{204}\text{Pb}$  are better than 0.8% (2RSE). We are able to present the first ever Pb isotope data from ~260 Ma Emeishan flood basalt olivine-hosted melt inclusions. They show the importance to do age correction which results in reducing the spread of data in old samples. The mean values of age-corrected  $^{208}\text{Pb}/^{206}\text{Pb}$  and  $^{207}\text{Pb}/^{206}\text{Pb}$  have 1.2% and 2.8% deviations from the uncorrected mean values, respectively. The method developed here provides a fast, precise and accurate *in-situ* Pb isotopic composition analysis, applicable not only to melt inclusions from young basalts, but also from old samples that require correction for U-Th decay.

## 59 Introduction

60 Melt inclusions are small parcels of melt trapped in crystals during magma  
61 evolution.<sup>1-5</sup> Compared to the whole rock, melt inclusions provide several advantages:

1  
2  
3  
4 62 1) if last equilibrated at higher pressures than those of eruption, melt inclusions can  
5 63 retain volatiles (H, C, Cl, S, F) and may provide the easiest way to measure these  
6 64 elements; 2) melt inclusions may represent primitive melts trapped in the early stages  
7 65 of magma evolution, and they may also preserve a wider diversity of melt  
8 66 compositions than are represented by the bulk host rocks; 3) in altered rocks, melt  
9 67 inclusions within resistant phenocryst phases may be protected from alteration,  
10 68 providing a useful method for producing less potentially ambiguous results to  
11 69 determine the composition of magmas in these whole rocks.<sup>4</sup> The Pb isotope  
12 70 composition of melt inclusions can provide important information on the origin of  
13 71 mafic lavas.<sup>3-6</sup> So far, Pb composition measurement of melt inclusions is mainly  
14 72 performed using Secondary Ion Mass Spectrometry (SIMS).<sup>3,6-9</sup> However, this  
15 73 approach is hampered by very high instrument cost (thus SIMS is not as widespread  
16 74 as LA-ICP-MS), limited analytical machine time for users, and high analysis cost. In  
17 75 recent years, laser ablation multiple-collector inductively-coupled-plasma mass  
18 76 spectrometry (LA-MC-ICP-MS) has become a powerful alternative method, as it can  
19 77 conduct *in situ* isotope analyses rapidly and at lower cost than SIMS. Because of these  
20 78 advantages, this technology has quickly been adopted for *in situ* Pb-isotope analysis.  
21 79 For example, Paul et al.<sup>10</sup> using a 93  $\mu\text{m}$  laser spot analyzed the Pb isotopic  
22 80 composition of glass standards. Kent<sup>11</sup> made a comparison between the Faraday cup  
23 81 and ion counting systems for Pb-isotope analysis and argued that the precision is  
24 82 strongly dependent on ion intensities. Souders and Sylvester<sup>12</sup> using a 40-99  $\mu\text{m}$  laser  
25 83 spot analyzed several glass standards with different Pb contents. Though analysis data  
26 84 from these studies have a good precision and accuracy, such large spot sizes or high  
27 85 repetition rates and strong laser energy (e.g. 93  $\mu\text{m}$ , 6 Hz, 5 J  $\text{cm}^{-2}$  of Paul et al.<sup>10,13</sup>;  
28 86 and 40-99  $\mu\text{m}$ , 10 Hz, 5 J  $\text{cm}^{-2}$  of Souders and Sylvester<sup>12</sup>) are difficult to apply to  
29 87 most melt inclusions because the inclusions will be fully penetrated in only a few  
30 88 seconds. Most melt inclusions are small and cannot be analyzed using a large laser  
31 89 spot (i.e., > 80  $\mu\text{m}$ ). In order to analyze Pb isotopes by LA-MC-ICP-MS in melt  
32 90 inclusions, the laser spot size, repetition rate and energy must be carefully adjusted to  
33 91 maximize the laser ablation time in order to obtain data of high precision. In this study,  
34 92 we have developed an analytical protocol for *in situ* measurements of Pb isotopes in  
35 93 relatively small (diameter > 40 $\mu\text{m}$ ) geological samples by LA-MC-ICP-MS. Using  
36 94 this protocol we undertook *in situ* analysis of Pb isotopes in several glass standards  
37 95 with different Pb contents (1.7-16  $\mu\text{g g}^{-1}$ ). In addition, we present Pb isotopic

1  
2  
3  
4 96 compositions of olivine-hosted melt inclusions from Cenozoic Hainan Island basalts  
5 97 erupted between ~17 Ma and ~0.1 Ma ago and end-Permian Emeishan flood basalts  
6  
7 98 erupted ~260Ma ago.  
8

9 99

## 10 **Instruments**

11  
12  
13 101 All analyses were performed using a Thermo Fisher Scientific Neptune Plus  
14 102 MC-ICPMS at the Guangzhou Institute of Geochemistry, Chinese Academy of  
15 103 Sciences. This machine is a double focusing multi-collector ICP-MS and has the  
16 104 capability of high mass resolution measurements in multiple collector mode. It is  
17 105 equipped with eight variable position Faraday cups and one fixed central Faraday cup,  
18 106 and eight ion counters (three of them are secondary electron multipliers and the others  
19 107 are compact discrete dynamic multipliers). This collector system can analyze isotopic  
20 108 ratios with a relative mass range of 17%, allowing simultaneous acquisition of ion  
21 109 signals ranging from mass  $^{202}\text{Hg}$  to  $^{238}\text{U}$ . This machine is also equipped with a newly  
22 110 designed large dry interface pump ( $100\text{ m}^3\text{ h}^{-1}$  pumping speed), which results in an  
23 111 increase in sensitivity. In addition, the newly designed interface cone assemblage  
24 112 consisting of a Jet sample cone and X skimmer cone (from Thermo Scientific) also  
25 113 significantly improves instrument sensitivity. This machine can work in static mode or  
26 114 peak jump mode, in our experiment, however only the static mode was used.

27  
28  
29 115 The laser ablation system, Resonetics RESolution M-50, includes: 1) a 193 nm  
30 116 Lambda Physik ComPex Pro 110 ArF excimer laser with a pulse width of ca. 20 ns; 2)  
31 117 a sample ablation stage that can hold four mounts at the same time; and 3) a high  
32 118 precision computer controlled sample positioning system. The laser spot size can vary  
33 119 from 5 to 380  $\mu\text{m}$ , the repetition rate from 1 to 20 Hz and the energy from 80 mJ to  
34 120 180 mJ. In order to weaken the laser energy, 25% and 50% energy attenuators are  
35 121 installed on the laser path which can change the laser energy density from  $\sim 2\text{ J cm}^{-2}$  to  
36 122  $18\text{ J cm}^{-2}$ . This allows samples with different sizes and different abundances of  
37 123 elements of interest to be measured. A “squid” smoothing device on the gas line to the  
38 124 ICP gives a smooth signal. The system can wash out 99% of the signal in less than 1.5  
39 125 seconds due to its innovative sample cell design. Helium is used as the carrier gas to  
40 126 enhance transport efficiency and minimize deposition of ablated material.<sup>14-16</sup> A small  
41 127 amount of  $\text{N}_2$  is added to the sample gas by a Y-shape connector to enhance the  
42 128 sample signal.  
43  
44  
45  
46  
47  
48  
49  
50  
51  
52  
53  
54  
55  
56  
57  
58  
59  
60

## 129 **Samples**

### 130 **Glass standards**

131 The standard glasses used in this study include: two NIST reference glasses, NIST  
132 612 ( $38.6 \mu\text{g g}^{-1} \text{Pb}$ )<sup>17</sup> and NIST 614 ( $2.32 \mu\text{g g}^{-1} \text{Pb}$ ),<sup>17</sup> two GSJ reference glasses,  
133 JB-1 ( $3.5 \mu\text{g g}^{-1} \text{Pb}$ )<sup>17</sup> and JB-2 ( $< 1 \mu\text{g g}^{-1} \text{Pb}$ ),<sup>18</sup> and three USGS reference glasses,  
134 BHVO-2G ( $1.7 \mu\text{g g}^{-1} \text{Pb}$ ),<sup>17</sup> NKT-1G ( $3.01 \mu\text{g g}^{-1} \text{Pb}$ )<sup>19</sup> and TB-1G ( $16 \mu\text{g g}^{-1} \text{Pb}$ ).<sup>20</sup>  
135 JB-1, JB-2, BHVO-2G and TB-1G are made from basalt powders and NKT-1G is  
136 made from peralkaline basalt powder, whereas NIST 612 and NIST 614 are synthetic  
137 standards.<sup>21-22</sup> Table 1 shows the major element composition of these standard glasses.  
138 Small chips of each selected standard glass were mounted in one-inch diameter epoxy  
139 resin mounts. The mount was polished to an even sample surface using diamond  
140 abrasive. To eliminate any potential surface contamination of the samples, each mount  
141 was cleaned in an ultrasonic bath with ~2% deperated nitric acid three times, rinsed  
142 with double-distilled Mili-Q water, and then the mount was dried with a nitrogen jet.

### 144 **Melt inclusions**

145 We handpicked olivine grains from crushed and sieved samples. To determine the Pb  
146 composition of melt inclusions, it is preferable to analyze a homogeneous glass rather  
147 than a mixture of various crystalline phases and residual glass.<sup>3-4,23</sup> In order to reduce  
148 the “matrix effect” between melt inclusions and glassy standards, prior to in situ Pb  
149 isotope analysis, the melt inclusions containing mixtures of crystals and glass require  
150 reheating and quenching in order to rehomogenize them as entirely glassy  
151 inclusions.<sup>1-3</sup> We reheated olivine grains and homogenized melt inclusions using  
152 1-atm furnaces at 1250 centigrade degree for 10 min in QFM-buffer condition, and  
153 then quenched and polished them until the melt inclusions were exposed at the surface.  
154 All sample preparation was performed at the melt inclusion laboratory in the State  
155 Key Laboratory of Isotope Geochemistry, Guangzhou institute of Geochemistry,  
156 Chinese Academy of Sciences (GIG-CAS). The preparation procedure of melt  
157 inclusions is described in detail by Ren et al.<sup>23</sup>

158 Statistics of nearly 1500 olivine-hosted melt inclusions from basalt-picrites from  
159 Hawaii (508), Hannuoba (North China craton, 343), Emeishan (296) and Hainan (301)  
160 show that about 42% of these melt inclusions have a diameter larger than  $40 \mu\text{m}$   
161 (short dimension). Only 9.5% of these melt inclusions have a diameter larger than 80

1  
2  
3  
4 162  $\mu\text{m}$  (Fig. 1). Whereas the Hainan island basalts were erupted in the Cenozoic and have  
5 163 a relatively young age, the Emeishan flood basalts are older having been erupted at  
6 164 the end of the Permian ( $\sim 260$  Ma) and the effect of U-Th decay on the Pb isotopic  
7 165 composition of their melt inclusions needs to be considered.  
8  
9

10 166

11  
12 **Analytical method**  
13

14 168 Hg may exist in Ar, He and  $\text{N}_2$  gases, and  $^{204}\text{Hg}$  has a significant isobaric interference  
15 169 on  $^{204}\text{Pb}$ .<sup>10,12,24</sup> To reduce  $^{204}\text{Hg}$  interference, three Au-coated glass wool Hg filters  
16 170 (VICI Metronics) were placed on the gas lines to the ablation cell to filter Hg from Ar,  
17 171 He and  $\text{N}_2$  gases. All gas tubes were rinsed with  $\sim 10\%$  purified nitric acid ( $\text{HNO}_3$ ) and  
18 172 rinsed again with double-distilled Milli-Q water. After this, the gas tubes were dried  
19 173 by ultra pure  $\text{N}_2$  gas flow. Other instrument components such as the cones and torch  
20 174 were washed with an ultrasonic cleaner in  $\sim 0.1\%$  distilled nitric acid for 20 minutes  
21 175 and then diluted by distilled Milli-Q water, before drying under ultra pure  $\text{N}_2$  gas  
22 176 flow.  
23  
24  
25  
26  
27  
28  
29

30 177 The gain factors for new Channeltrons need a “burn-in” period (several months to  
31 178 years) for stabilization.<sup>20,24</sup> The instrument used in our study had run for more than  
32 179 one year when we performed these analyses. Over this time the gain factors for ion  
33 180 counters (ICs) used in this study have become stable. Prior to each analytical period,  
34 181 the relative yield values for each IC were determined referenced to IC1 under peak  
35 182 jump mode. After an  $\sim 40$ -minute warm-up period, gas flow, torch position, lens focus  
36 183 potentials, peak overlap and peak center were checked and adjusted. Then the yield  
37 184 values were measured in solution mode with an integration time of 4.194 s. A low  
38 185  $^{238}\text{U}$  signal ( $\sim 3\text{mv}/187500\text{cps}$ ) from the Neptune tune solution was used. The  $^{238}\text{U}$   
39 186 signal entered in the eight ICs sequentially under different magnetic fields. The yield  
40 187 values measurement included 10 blocks, and each block had 10 cycles. The yield  
41 188 values for each IC were then determined by normalizing the measured signal  
42 189 intensities for each IC to IC1. If the relative yield values are not within 80% of IC1,  
43 190 the operation voltage on the IC is improved. During almost 2 hours relative yield  
44 191 determination for each IC, the uncertainty of the yield value for each IC was less than  
45 192 1.5% (2RSD).  
46  
47  
48  
49  
50  
51  
52  
53  
54  
55  
56  
57

58 193 The gas flow, torch position, lens focus potentials, peak overlap and peak center  
59 194 were checked and adjusted to achieve a typical  $^{208}\text{Pb}$  sensitivity of 95000 cps per  $\mu\text{g}$   
60

1  
2  
3  
4 195  $\text{g}^{-1}$  Pb with standard cones assemblage for *in situ* analyses of NIST 614 with a 32  $\mu\text{m}$   
5 196 and 10 Hz repetition rate laser spot. The  $^{208}\text{Pb}$  signals of all samples were limited  
6 197 larger than 100000 cps to ensure a reasonable analytical precision and not more than  
7 198 500000 cps to prolong the lifetime of the ICs and to limit the ICs drift through  
8 199 adjusting laser parameters. Under the normal 45  $\mu\text{m}$  laser spot used in our study,  
9 200 100000-500000 cps  $^{208}\text{Pb}$  intensity corresponds to about 1-6  $\mu\text{g g}^{-1}$  Pb content which  
10 201 ensures a reasonable analytical precision. However, if the sample has Pb content more  
11 202 than 6  $\mu\text{g g}^{-1}$ , we can change the laser spot to smaller size (from 45  $\mu\text{m}$  to 33  $\mu\text{m}$ ) to  
12 203 reduce the signal intensity. During our experiment, gas blanks for  $^{202}\text{Hg}$  and  $^{208}\text{Pb}$   
13 204 were  $\sim 4000$  cps and  $< 100$  cps when using the standard cones assemblage. When using  
14 205 the Jet sample cone and X skimmer cone, the instrument sensitivity was improved and  
15 206 the intensities of gas blanks for  $^{202}\text{Hg}$  and  $^{208}\text{Pb}$  rose to  $\sim 4000$ -9000 cps and  $< 200$  cps.  
16 207 Typical instrument operating parameters and the collector configuration for the  
17 208 analysis of Pb isotopes are listed in Tables 2 and 3.

18 209 All time-resolved raw data were exported from the MC-ICP-MS in ASCII format  
19 210 with Neptune Plus software and processed off-line using a spreadsheet program  
20 211 created by the authors. First, the mean gas background intensities were subtracted  
21 212 from the raw time-resolved signal intensities for each isotope. Then the isobaric  
22 213 interference of  $^{204}\text{Hg}$ , which was calculated with the measured  $^{202}\text{Hg}$  intensity and the  
23 214 natural  $^{204}\text{Hg}/^{202}\text{Hg}$  ratio (0.2301<sup>25</sup>), was subtracted from  $^{204}(\text{Pb}+\text{Hg})$  to obtain the net  
24 215  $^{204}\text{Pb}$  signal intensity. Finally all isotope ratios were calculated and corrected for mass  
25 216 bias and instrumental drift with a standard-sample-standard bracketing method and  
26 217 any outliers ( $> \pm 2\text{SD}$ ; standard deviation) were excluded. The following gives a detail  
27 218 description of the data reduction techniques.

### 28 219

### 29 220 **Mass bias correction**

30 221 Among the four Pb isotopes ( $^{208}\text{Pb}$ ,  $^{207}\text{Pb}$ ,  $^{206}\text{Pb}$  and  $^{204}\text{Pb}$ ),  $^{208}\text{Pb}$ ,  $^{207}\text{Pb}$  and  $^{206}\text{Pb}$  are  
31 222 derived from the radioactive decay of U and Th and only  $^{204}\text{Pb}$  is an invariant isotope.  
32 223 As a result for Pb isotope analysis, there is no invariant isotope pair to make a mass  
33 224 bias correction as is performed in Sr, Nd and Hf isotope systems. One strategy is to  
34 225 aspirate a Tl tracer solution during laser analysis to monitor Pb fractionation.<sup>26-27</sup>  
35 226 Another strategy is to use standard materials to make external corrections.<sup>10-12</sup>  
36 227 Because the configuration of the ion counters in the instrument used in this study do  
37 228 not allow the signals of Tl, Pb and Hg to be received simultaneously the mass bias



229 correction was performed with the later method. The Pb isotope measurement of  
230 every unknown sample was preceded and followed by once measurement of standard  
231 glass, and using the follow equation:

$$S_c = \frac{S_m}{(R_{m1} + R_{m2}) / 2 / R} \quad (1)$$

233 where  $S_m$  is the measured value on the unknown sample;  $R_{m1}$  and  $R_{m2}$  are the  
234 measured values on the analysis of the standard glass preceding and following the  
235 unknown, respectively; and  $R$  is preferred reference value, the final corrected value  
236 ( $S_c$ ) was calculated.

## 238 Results and discussion

### 239 Measurement of standard solutions

240 NBS 981 standard solution and the Neptune standard solution were used to evaluate  
241 the accuracy and precision of the instrument during Pb isotope analysis. NBS 981 was  
242 used as an external standard whereas the Neptune solution was the “unknown sample”.  
243 The two solutions were analyzed in turn and the Neptune solution’s Pb isotope ratios  
244 were corrected using Eq 1. We measured two Neptune solutions with different Pb  
245 contents (one where  $^{208}\text{Pb}$  signal intensity was 190000 cps (counts per second) and the  
246 other where it was 32000 cps), and using two different integration times (0.131 and  
247 1.049 s). An integration time of 0.131 s allowed 600 cycles of data to be obtained;  
248 1.049 s allowed 90 cycles of data to be obtained (Supplementary data S1).

249 The results show that  $^{208}\text{Pb}/^{206}\text{Pb}$  and  $^{207}\text{Pb}/^{206}\text{Pb}$  of the Neptune solution with  
250 190000 cps  $^{208}\text{Pb}$  intensity have external precisions (2 relative standard deviation,  
251 2RSD;  $n = 40$ ) better than 0.15% and both are within 0.02% of the preferred values.  
252  $^{20x}\text{Pb}/^{204}\text{Pb}$  ( $x = 6, 7$  or  $8$ ) of the same solution have external precisions better than  
253 0.31% (2RSD) and are within 0.05% of the preferred values. The Pb isotope ratios of  
254 the Neptune solution with  $^{208}\text{Pb}$  intensity of 32000 cps are just slightly less precise  
255 than that of the other solution (For example, with an integration time of 1 s the precise  
256 of  $^{207}\text{Pb}/^{206}\text{Pb}$  of the solution with 190000 cps  $^{208}\text{Pb}$  intensity is 0.0006 (2SD) and  
257 under the same instrument condition, the precision of the solution with 32000 cps  
258  $^{208}\text{Pb}$  intensity is 0.0014 (2SD)). Under the same signal intensity, the precision of data  
259 with an integration time of 1 s are slightly better than those with an integration time of  
260 0.131 s. The internal precision of data for the solution with 32000 cps  $^{208}\text{Pb}$  intensity

1  
2  
3 261 is twice as large as those for the solution with a 190000 cps  $^{208}\text{Pb}$  intensity. This  
4  
5 262 indicates that prolonging integration time and raising signal intensity can improve  
6  
7 263 analysis precision. The instrument has good stability and data reproducibility and the  
8  
9 264 external correction used to correct instrument drift and mass bias is robust.  
10  
11 265

### 266 **Correlation between internal precision and ablation time**

12  
13  
14 267 To better understand the relationship between internal precision and ablation time we  
15  
16 268 analyzed the Pb isotopic composition of NKT-1G over different ablation times (5, 10,  
17  
18 269 15... 60 s). Three analyses were performed using each ablation time and then  
19  
20 270 averaged (Fig. 2). As ablation time increases the precision improves. When the  
21  
22 271 ablation time is less than 20 s, the precision deteriorates quickly (the standard errors  
23  
24 272 (SE) of  $^{208}\text{Pb}/^{204}\text{Pb}$  and  $^{208}\text{Pb}/^{206}\text{Pb}$  are larger than 0.17, 0.0012 respectively), whereas  
25  
26 273 above 30 s there is little improvement. Based on this fact, an ablation time of 30 s was  
27  
28 274 chosen to ensure data with good internal precision and that most melt inclusions  
29  
30 275 larger than 40  $\mu\text{m}$  in diameter would not fully penetrated.

31  
32 276 Using the standard sample cone and skimmer cone, the signal intensity of samples  
33  
34 277 with low Pb content ( $<10 \mu\text{g g}^{-1}$ ) are relatively low and the precisions of ratios  
35  
36 278 involving  $^{204}\text{Pb}$  are poor. The assemblage of a Jet sample cone and X skimmer cone  
37  
38 279 can significantly improve the sample signal.<sup>28-29</sup> As a result both the standard cones  
39  
40 280 assemblage and the Jet and X cones assemblage were used to measure the same  
41  
42 281 samples and compared to assess data precision and accuracy.  
43  
44 282

### 45 **Standard cones assemblage**

46  
47 284 In order to compare our results with previous LA-MC-ICPMS results at a similar  
48  
49 285 signal intensity, Pb isotopes of NIST 614 and NKT-1G were analyzed using a standard  
50  
51 286 cones assemblage and laser parameters optimized to obtain the same signal intensities  
52  
53 287 as in previous studies.

54  
55 288 The laser parameters were adjusted (spot size: 32  $\mu\text{m}$ ; repetition rate: 10 Hz;  
56  
57 289 energy: 100 mJ; energy density: 9  $\text{J cm}^{-2}$ , integration time: 1.049 s) to achieve 220000  
58  
59 290 cps  $^{208}\text{Pb}$  signal intensity (5800 cps for  $^{204}\text{Pb}$ ) for NIST 614 ( $2.32 \mu\text{g g}^{-1}$  Pb), similar  
60  
291 to that of MPI-T1-G in Souders and Sylvester<sup>12</sup> ( $\sim 240000$  cps) (Table 4 and Fig. 3).  
292 The data in six days over two month shows the external precisions (2RSD) of  
293  $^{208}\text{Pb}/^{206}\text{Pb}$ ,  $^{207}\text{Pb}/^{206}\text{Pb}$ ,  $^{207}\text{Pb}/^{204}\text{Pb}$ ,  $^{208}\text{Pb}/^{204}\text{Pb}$  and  $^{206}\text{Pb}/^{204}\text{Pb}$  are 0.29%, 0.41%,  
294 0.98%, 0.97% and 0.93%, respectively; a little worse than those reported for

1  
2  
3  
4 295 MP1-T1-G by Souders and Sylvester<sup>12</sup> (Table 5). This may be caused by the lower  
5  
6 296 signal intensity in this study. The accuracy for  $^{208}\text{Pb}/^{206}\text{Pb}$  and  $^{207}\text{Pb}/^{206}\text{Pb}$  are better  
7  
8 297 than 0.07% and for  $^{20x}\text{Pb}/^{204}\text{Pb}$ , better than 0.45%. Using a laser spot of 32  $\mu\text{m}$  spot,  
9  
10 298 10 Hz repetition rate and 80 mJ energy with a 50% energy attenuator (4 J  $\text{cm}^{-2}$  energy  
11  
12 299 density), NKT-1G (3.01  $\mu\text{g g}^{-1}$  Pb) has a signal intensity of 90000 cps for  $^{208}\text{Pb}$  (2400  
13  
14 300 cps for  $^{204}\text{Pb}$ ), which is almost the same as that for MPI-ML3B-G in Souders and  
15  
16 301 Sylvester<sup>12</sup> ( $\sim 86000$  cps). The precisions and accuracies for  $^{208}\text{Pb}/^{206}\text{Pb}$  and  
17  
18 302  $^{207}\text{Pb}/^{206}\text{Pb}$  are  $\sim 0.44\%$  (2RSD) and  $\sim 0.10\%$  respectively, whereas for  $^{20x}\text{Pb}/^{204}\text{Pb}$ ,  
19  
20 303 they are  $\sim 1.70\%$  (2RSD) and  $\sim 0.60\%$  (Table 4) which show an improved accuracy  
21  
22 304 and precision compared to the result of MPI-ML3B-G in Souders and Sylvester<sup>12</sup>  
23  
24 305 (Table 5).

25  
26 306 In order to measure melt inclusions with diameters less than 30  $\mu\text{m}$ , we propose a  
27  
28 307 23  $\mu\text{m}$  laser spot size, 3 Hz repetition rate and 80 mJ energy with a 50% energy  
29  
30 308 attenuator (energy density is 4 J  $\text{cm}^{-2}$ ). Under these laser conditions, NIST 614 and  
31  
32 309 TB-1G were measured (n=110). The  $^{208}\text{Pb}$  signal for NIST 614 is about 22000 cps  
33  
34 310 (600 cps for  $^{204}\text{Pb}$ ), the precisions (2RSD) for  $^{208}\text{Pb}/^{206}\text{Pb}$ ,  $^{207}\text{Pb}/^{206}\text{Pb}$ ,  $^{207}\text{Pb}/^{204}\text{Pb}$ ,  
35  
36 311  $^{208}\text{Pb}/^{204}\text{Pb}$  and  $^{206}\text{Pb}/^{204}\text{Pb}$  are 0.64%, 0.79%, 4.05%, 4.25% and 4.17% respectively,  
37  
38 312 and their accuracies are 0.25%, 0.03%, 0.51%, 0.36% and 0.36%, respectively (Table  
39  
40 313 4 and Fig. 4). Obviously, because the sample signal is much lower, the precisions of  
41  
42 314 ratios involving  $^{204}\text{Pb}$  are much worse and the accuracies a little worse compared to  
43  
44 315 the normal set up. For TB-1G, however, the  $^{208}\text{Pb}$  signal intensity is relatively high  
45  
46 316 (90000 cps signal intensity for 16  $\mu\text{g g}^{-1}$  total Pb) resulting in improved precisions and  
47  
48 317 accuracies for Pb isotope ratios. The precisions and accuracies for  $^{208}\text{Pb}/^{206}\text{Pb}$  and  
49  
50 318  $^{207}\text{Pb}/^{206}\text{Pb}$  are  $\sim 0.4\%$  (2RSD) and  $\sim 0.20\%$ . For  $^{20x}\text{Pb}/^{204}\text{Pb}$ , the precisions and  
51  
52 319 accuracies are  $\sim 1.60\%$  and  $\sim 0.40\%$ , respectively.

### 320 321 **Jet sample cone and X skimmer cone assemblage**

322 Compared to the standard sample cone, using the Jet sample cone and X skimmer  
323  
324 323 cone together with a large dry interface pump can improve the signal intensity  
325  
326 324 significantly. With a laser spot size of  $\sim 23 \mu\text{m}$ , repetition rate of 3 Hz; energy density  
327  
328 325 of 4 J  $\text{cm}^{-2}/2.3 \text{ J cm}^{-2}$  and a 50%/25% energy attenuator, BHVO-2G, NKT-1G and  
326  
327 326 TB-1G were analyzed with the Jet sample cone and X skimmer cone. The results  
328  
329 327 show that with increasing sample Pb content data precision improves (Table 4).  
330  
331 328 BHVO-2G, which has the lowest Pb content among the three glasses, had the lowest

1  
2  
3  
4 329 signal intensity under these laser conditions (~55000 cps and 1500 cps for  $^{208}\text{Pb}$  and  
5 330  $^{204}\text{Pb}$ ). This results in poor precision for ratios involving  $^{204}\text{Pb}$ , larger than 5.0%  
6  
7 331 (2RSD). NKT-1G, with  $3.01 \mu\text{g g}^{-1}$  total Pb, shows better precisions compared to  
8  
9 332 BHVO-2G. The precisions for ratios involving  $^{204}\text{Pb}$  are a little larger than 3.0% and  
10 333 for  $^{208}\text{Pb}/^{206}\text{Pb}$  and  $^{207}\text{Pb}/^{206}\text{Pb}$  they are better than 0.40% (2RSD). TB-1G, which has  
11  
12 334 the highest signal intensity (~420000 cps and 11000 cps for  $^{208}\text{Pb}$  and  $^{204}\text{Pb}$ ), has  
13  
14 335 precisions ~1.0% or better for ratios involving  $^{204}\text{Pb}$ , and 0.19% and 0.16% (2RSD)  
15  
16 336 for  $^{208}\text{Pb}/^{206}\text{Pb}$  and  $^{207}\text{Pb}/^{206}\text{Pb}$ , respectively; most of these ratios are within 0.30% of  
17  
18 337 the preferred values. Compared to standard cones, using the Jet sample cone and X  
19  
20 338 skimmer cone for TB-1G results in significant improvements in precision (Table 4).

21 339 Under the same laser conditions, we compared single spot analyses for NIST 614  
22  
23 340 using the standard cones assemblage with one using the Jet and X cones. Using the  
24  
25 341 standard cones, the  $^{208}\text{Pb}$  signal intensity for NIST 614 is about 22000 cps, whereas  
26  
27 342 using the Jet and X cones it increases to 65000 cps (Fig. 5). It is clear that the  
28  
29 343 variations of these Pb isotope ratios using the standard cones assemblage are larger  
30  
31 344 than those using the Jet and X cone assemblage. For example, the internal precision  
32  
33 345 (relative standard error, RSE) of  $^{208}\text{Pb}/^{204}\text{Pb}$  using the standard cones assemblage  
34  
35 346 (1.6%) is two time larger than that using the Jet and X cones assemblage (0.8%) (Fig.  
36  
37 347 5).

38 348 Compared to the standard cones assemblage, the Jet sample cone and X skimmer  
39  
40 349 cone assemblage can improve the external precisions of *in situ* Pb isotope ratios  
41  
42 350 significantly (Fig. 6a, b). Using the Jet and X cones, under the same laser ablation  
43  
44 351 conditions, the precisions for almost all the samples are improved by at least a factor  
45  
46 352 of two compared to using the standard cones. For example, using the standard cones  
47  
48 353 with a  $24 \mu\text{m}$  laser spot the  $^{208}\text{Pb}$  signal intensity for TB-1G is ~140000cps and the  
49  
50 354  $^{208}\text{Pb}/^{206}\text{Pb}$  and  $^{208}\text{Pb}/^{204}\text{Pb}$ 's precisions are 0.38% and 2.26% (2RSD). When using  
51  
52 355 the Jet and X cones, the  $^{208}\text{Pb}$  signal intensity for TB-1G is improved to ~420000cps,  
53  
54 356 and the precisions are improved to 0.19% and 1.04% (2RSD) respectively.

55 357

### 358 **Correlation of external precision and signal intensity**

56 359 In order to obtain a more accurate relationship between data precision and signal  
57  
58 360 intensity, we measured samples with different Pb contents under different laser  
59  
60 361 ablation conditions. The results show that the precisions using the standard cones  
362 362 assemblage and the Jet and X cones assemblage are almost identical at the same

1  
2  
3  
4 363 signal intensity (since the precisions of  $^{207}\text{Pb}/^{204}\text{Pb}$  and  $^{206}\text{Pb}/^{204}\text{Pb}$  are similar to the  
5 364 precision of  $^{208}\text{Pb}/^{204}\text{Pb}$ , only the data of  $^{208}\text{Pb}/^{204}\text{Pb}$  are displayed in Fig. 6). However,  
6  
7 365 using the Jet and X cones can improve signal intensity by up to two times compared  
8  
9 366 to using the standard cones, which greatly improves precision. For example, using the  
10 367 standard cones, with a 45  $\mu\text{m}$  laser spot, the  $^{208}\text{Pb}$  signal intensity of BHVO-2G is  
11 368 only  $\sim 48000$  cps and the external precisions for  $^{208}\text{Pb}/^{206}\text{Pb}$  and  $^{208}\text{Pb}/^{204}\text{Pb}$  are 0.44%  
12 369 and 2.07% (2RSD) (Fig. 6c, d). When using the Jet and X cones, under the same laser  
13 370 ablation conditions,  $^{208}\text{Pb}$  signal intensity of BHVO-2G rises to  $\sim 134000$  cps and the  
14 371 precisions for  $^{208}\text{Pb}/^{206}\text{Pb}$  and  $^{208}\text{Pb}/^{204}\text{Pb}$  are improved to 0.14% and 1.04%,  
15 372 respectively. The precision for our measured  $^{208}\text{Pb}/^{206}\text{Pb}$  ratios are much better than  
16 373 the results of Souders and Sylvester<sup>12</sup> while for  $^{208}\text{Pb}/^{204}\text{Pb}$  the precision is similar at  
17 374 the same signal intensity (Fig. 6c, d). This may be caused by the intensity of the  
18 375  $^{204}(\text{Hg}+\text{Pb})$  background, which also was higher with the Jet and X cones assemblage  
19 376 ( $\sim 4000$ - $9000$  cps). From the discussion above we know that under the same laser  
20 377 ablation conditions the Jet and X cones assemblage significantly improves the  
21 378 precision compared to the standard cones for the same sample. So replacing the  
22 379 standard cones with Jet and X cones will provide much more precise Pb isotope ratio  
23 380 data compared to the setup of Souders and Sylvester.<sup>12</sup>

24  
25  
26  
27  
28  
29  
30  
31  
32  
33  
34  
35 381 Obviously, the precision for experimental data is controlled by many factors, such  
36 382 as sample signal, laser ablation time, instrument condition and gas blank, and the  
37 383 sample signal is governed by the content of the element of interest, laser ablation  
38 384 parameters (spot size, repetition rate and energy) and instrument sensitivity. For a  
39 385 given sample (such as a melt inclusion), the content of the element of interest is fixed,  
40 386 while for a given laboratory, the instrument sensitivity and gas blank are relatively  
41 387 stable, and thus the instrumental parameters will be the main factor controlling data  
42 388 precision. Therefore optimization of the instrument parameters for a given sample is  
43 389 crucial. In analyzing inclusions a balance must be obtained between parameter  
44 390 settings that create a high enough signal intensity to have a reasonable precision, but  
45 391 do not result in the laser ablating all the way through the inclusion.  
46  
47  
48  
49  
50  
51  
52  
53  
54  
55

### 56 393 **Measurement of natural melt inclusions**

57 394 We measured Pb isotopes in 429 olivine-hosted melt inclusions from the Cenozoic  
58  
59 395 Hainan Island basalts (219) and the end-Permian Emeishan flood basalts (210).  
60

1  
2  
3 396 Olivine-hosted melt inclusions are mafic and the compositions and Pb contents are  
4 similar to those of NKT-1G and BVHO-2G. Thus both standard glasses have  
5 397 similar to those of NKT-1G and BVHO-2G. Thus both standard glasses have  
6 relatively small matrix effects compared to the measured melt inclusions. NKT-1G  
7 398 relatively small matrix effects compared to the measured melt inclusions. NKT-1G  
8 was selected as the external standard bracketing each melt inclusion measurement.  
9 399 was selected as the external standard bracketing each melt inclusion measurement.  
10 400 BHVO-2G was analyzed after every five melt inclusion measurements to monitor  
11 instrument drift. At the beginning of each analysis session, five pairs of NKT-1G and  
12 401 instrument drift. At the beginning of each analysis session, five pairs of NKT-1G and  
13 BHVO-2G were analyzed. After making sure that the corrected Pb isotope ratios of  
14 402 BHVO-2G were analyzed. After making sure that the corrected Pb isotope ratios of  
15 BHVO-2G are within analytical error of the preferred reference values the Pb isotopic  
16 403 BHVO-2G are within analytical error of the preferred reference values the Pb isotopic  
17 404 composition of the melt inclusions were measured.  
18  
19 405

### 406 **Olivine-hosted melt inclusions from Hainan island basalts**

407 At first, we adjusted the laser to a 23  $\mu\text{m}$  spot size, 3Hz repetition rate, 80 mJ  
408 energy with a 50% energy attenuator ( $4 \text{ J cm}^{-2}$  energy density) to analyze melt  
409 inclusions from the Hainan island basalts. However, the measurement results showed  
410 that the signal intensity of the melt inclusions are very low (the intensity of  $^{208}\text{Pb}$  was  
411 about 5000-130000 cps (1300-3400 cps for  $^{204}\text{Pb}$ ), mostly 20000-80000 cps, and the  
412 Pb content was estimated to be about  $0.1\text{-}2.5 \mu\text{g g}^{-1}$ ) under these conditions. At such  
413 low intensities the internal precisions of the data for melt inclusions were poor  
414 (internal precisions of  $^{208}\text{Pb}/^{206}\text{Pb}$  for most inclusions were larger than 0.40% (2RSE)).  
415 To improve the sample signal intensity, we increased the laser spot size to 45  $\mu\text{m}$ . In  
416 order to get enough data before the melt inclusions were fully penetrated, a 25%  
417 energy attenuator was used. Melt inclusions with diameter larger than 40  $\mu\text{m}$  were  
418 analyzed. Under such laser conditions, the sample signal intensity was improved by a  
419 factor of two and the internal precision was significantly improved (internal  
420 precisions of  $^{208}\text{Pb}/^{206}\text{Pb}$  for most inclusions were less than 0.25% (2RSE)). The  
421 average  $^{208}\text{Pb}/^{206}\text{Pb}$  ratios of BHVO-2G over 3 days are within 0.20% of the preferred  
422 values and the ratios involving  $^{204}\text{Pb}$  are within 1.0% of the preferred values (Table 6  
423 and Fig. 7). Melt inclusion YX-11-1(3)-8 was large enough ( $\sim 150\mu\text{m}$ ) to be ablated  
424 three times. These duplicate measurements show excellent agreement. The precisions  
425 for  $^{208}\text{Pb}/^{206}\text{Pb}$  and  $^{207}\text{Pb}/^{206}\text{Pb}$  are better than 0.2% (2SD) and for  $^{208}\text{Pb}/^{204}\text{Pb}$  are  
426 better than 1.3% (2SD) (Table 6).  
427

### 428 **Olivine-hosted melt inclusions from the Emeishan flood basalts**

429 210 olivine-hosted melt inclusions from 9 Emeishan basalts were analyzed with a 45

1  
2  
3  
4 430  $\mu\text{m}$  laser spot (This means about 20-30 melt inclusions in each rock sample were  
5  
6 431 analyzed). Because the Emeishan flood basalts erupted at  $\sim 260$  Ma the effect of U-Th  
7  
8 432 decay on Pb isotope ratios must be corrected. The following protocol was adopted.  
9  
10 433 The mean gas background intensities were subtracted from the time-resolved signal  
11  
12 434 intensities for each isotope. Then U/Pb and Th/Pb were corrected for elemental  
13  
14 435 fractionation related to pit depth (referred to as downhole fractionation) and the mass  
15  
16 436 bias correction was followed. As shown in many zircon U-Pb dating studies,<sup>30-33</sup> the  
17  
18 437 downhole fractionation of U/Pb is linear with time. In our experiment, the  
19  
20 438 within-analysis laser induced downhole fractionation of  $^{238}\text{U}/^{206}\text{Pb}$  and  $^{232}\text{Th}/^{206}\text{Pb}$   
21  
22 439 were corrected by applying a linear regression through all measured ratios. Fig. 8  
23  
24 440 shows typical time-resolved data acquired during laser ablation of the external  
25  
26 441 standard NKT-1G. During the first 22 s, the gas blank was measured with the laser off,  
27  
28 442 followed by 30 s of sample measurement with laser on. The valid data begins at 25 s  
29  
30 443 and ends at 55 s. During the laser ablation, as the ablation pit deepens,  $^{238}\text{U}/^{206}\text{Pb}$  and  
31  
32 444  $^{232}\text{Th}/^{206}\text{Pb}$  decrease linearly with time. Pb is more volatile over U and this leads to  
33  
34 445 preferential volatilization of Pb over U and Th during laser ablation.<sup>32</sup> With the  
35  
36 446 process of laser ablation, the ablation pit gets deeper and the laser energy reaching the  
37  
38 447 sample surface gets less which leads to a stronger Pb and U/Th fractionation. This  
39  
40 448 means the U/Pb and Th/Pb ratios will get smaller and smaller with the process of laser  
41  
42 449 ablation. We used a linear correlation to calculate both  $^{238}\text{U}/^{206}\text{Pb}$  and  $^{232}\text{Th}/^{206}\text{Pb}$   
43  
44 450 ratios when the valid data started to be collected (i.e., at 25 s). After the mass bias  
45  
46 451 correction, it is necessary to use U-Pb and Th-Pb decay functions to calculate the Pb  
47  
48 452 isotope ratios of the melt inclusions from the Emeishan flood basalts to the time when  
49  
50 453 they were formed. Due to the low  $^{204}\text{Pb}$  intensity of the Emeishan melt inclusions and  
51  
52 454 resultant poor precision, the ratios involving  $^{204}\text{Pb}$  were not used. Only the  $^{208}\text{Pb}/^{206}\text{Pb}$   
53  
54 455 and  $^{207}\text{Pb}/^{206}\text{Pb}$  were calculated to their initial values. The method for calculating  
55  
56 456 initial lead isotope ratios is given in Supplemental data S2.

57  
58 457 The  $^{238}\text{U}/^{206}\text{Pb}$  and  $^{232}\text{Th}/^{206}\text{Pb}$  for the uncorrected Pb isotope ratios are  
59  
60 458 0.1927-1.3334 and 0.5570-5.0304 respectively. Their  $^{208}\text{Pb}/^{206}\text{Pb}$  and  $^{207}\text{Pb}/^{206}\text{Pb}$   
459  
460 459 range from 2.0275-2.1014 and 0.8070-0.8426, with mean values 2.0671 and 0.8215,  
461  
462 460 respectively (Fig. 9 and Supplementary data S3). After U-Th correction, the  
463  
464 461  $^{208}\text{Pb}/^{206}\text{Pb}$  and  $^{207}\text{Pb}/^{206}\text{Pb}$  of the Emeishan melt inclusions ranging from  
465  
466 462 2.0610-2.1179 and 0.8330-0.8617, with means of 2.0911 and 0.8445, have deviations  
467  
468 463 of 1.2% and 2.8% with the uncorrected Pb isotope ratios, respectively. This shows the

1  
2  
3 464 necessity to perform age-corrections for old samples.  
4  
5 465  
6

### 7 466 **Comparison with previous studies**

8  
9 467 Table 5 presents a summary of results obtained in previous studies, which can be  
10 468 compared with our results in Table 4 and 6. The detectors used by Paul et al.<sup>10</sup> and  
11 469 Kent<sup>11</sup> to measure <sup>208</sup>Pb, <sup>207</sup>Pb and <sup>206</sup>Pb are faraday cups that have much lower  
12 470 sensitivities than ICs. In order to achieve the required signal intensity, both studies  
13 471 used quite large laser spots and 60 s ablation time; these conditions are only suitable  
14 472 for analyzing large melt inclusions. Souders and Sylvester<sup>12</sup> used a smaller laser spot  
15 473 but the laser repetition rate of 10 Hz that they used is too high for most melt inclusion  
16 474 measurements. Using a 24 μm laser spot with a 3 Hz repetition rate, the external  
17 475 precisions for <sup>208</sup>Pb/<sup>206</sup>Pb and <sup>207</sup>Pb/<sup>206</sup>Pb for almost all standard glasses measured in  
18 476 our study (Fig. 6) are better than the results obtained by SIMS in the study of Saal et  
19 477 al.<sup>7</sup> and are comparable to those obtained in the study of Souders and Sylvester.<sup>12</sup> The  
20 478 laser condition (spot size: 45 μm spot, repetition rate: 3Hz and 80 mJ energy with a  
21 479 25% energy attenuator (~2.3 J cm<sup>-2</sup> energy density)) used to analyze natural melt  
22 480 inclusions in this study can be used to measure Pb isotopes in most melt inclusions  
23 481 larger than 40 μm. Compared to the 93 μm laser spot used by Paul et al.,<sup>13</sup> our method  
24 482 makes it possible for much smaller melt inclusions to be analyzed for Pb isotopes.  
25 483 What is more, our method collects U and Th data along with the Pb isotopes  
26 484 permitting age-corrections to be performed in melt inclusions from ancient lavas  
27 485 which results in reducing the spread of data (Fig. 9). Considering these facts, we  
28 486 suggest that the analytical protocol presented here offers an improvement in Pb  
29 487 isotope analysis compared to previous studies.  
30  
31  
32  
33  
34  
35  
36  
37  
38  
39  
40  
41  
42  
43  
44  
45  
46  
47

### 48 489 **Conclusions**

49  
50 490 Under the same laser ablation condition, using the Jet sample cone and X skimmer  
51 491 cone can improve sample signal intensity by up to 2 times compared to using standard  
52 492 cones and the precisions of Pb isotopic ratios can be improved at least by a factor of  
53 493 two. The precision of collected data is controlled by many factors. However, for a  
54 494 specific sample and laboratory, the laser condition, which has a critical effect on the  
55 495 sample signal intensity, acts as the main factor controlling the data precision.  
56 496 Therefore optimizing the laser parameters for a specific sample is vital. Optimized  
57  
58  
59  
60



1  
2  
3  
4 497 laser parameters to analyze Pb isotopes in melt inclusions, using a Jet sample and X  
5 498 skimmer cone, give  $^{208}\text{Pb}$  signal intensity > 200000 cps, external precisions of ratios  
6 499 involving  $^{204}\text{Pb}$  better than 1.3% (2RSD), and precisions of  $^{208}\text{Pb}/^{206}\text{Pb}$  and  
7 500  $^{207}\text{Pb}/^{206}\text{Pb}$  better than 0.23% (2RSD). Measurement of melt inclusions from old  
8 501 samples, such as the ~260 Ma Emeishan basalts, shows that it is important to conduct  
9 502 age-corrections in such samples. Compared to previous studies, the laser condition  
10 503 (spot size: 45  $\mu\text{m}$  spot, repetition rate: 3Hz and 80 mJ energy with a 25% energy  
11 504 attenuator (~2.3 J  $\text{cm}^{-2}$  energy density)) used in our protocol is more suitable for most  
12 505 melt inclusion Pb isotope measurements. The method we have developed can provide  
13 506 fast, precise and accurate *in-situ* Pb composition analysis, not only for young melt  
14 507 inclusions, but also for old samples that require age-correction for U-Th decay. To  
15 508 improve the precision of  $^{20x}\text{Pb}/^{204}\text{Pb}$  for samples with very low Pb content (< 1 $\mu\text{g g}^{-1}$ ),  
16 509 further study is needed to improve the sample signal intensity and reduce the Hg gas  
17 510 blank.  
18  
19  
20  
21  
22  
23  
24  
25  
26  
27  
28  
29

### 30 512 **Acknowledgements**

31 513 We would like to thank Wu Lei for kind assistance with sample preparations and  
32 514 LA-MC-ICP-MS measurements. The authors thank three anonymous reviewers for  
33 515 their critical and constructive comments to improve this manuscript. The authors  
34 516 gratefully acknowledge the financial support from the National Basic Research  
35 517 Program of China (2011CB808903), the National Science Foundation of China  
36 518 (91214202, 41172064), and the “hundred talent project” of Chinese Academy of  
37 519 Sciences.  
38  
39  
40  
41  
42  
43  
44  
45

### 46 521 **References**

- 47 522 1. A. V. Sobolev, *Petrol.*, 1996, 4, 209-220.  
48 523 2. L. V. Danyushevsky, F. N. Della-Pasqua and S. Sokolov, *Contrib. Mineral.*  
49 524 *Petrol.*, 2000, 138, 68-83.  
50 525 3. E. Hauri, *Chem. Geol.*, 2002, 183, 115-141.  
51 526 4. A. J. R. Kent, *Rev. Mineral. Geochem.*, 2008, 69, 273-331.  
52 527 5. V. S. Kamenetsky, A. A. Gurenko and A. C. Kerr, *Geology*, 2010, 38, 1003-1006.  
53 528 6. A. E. Saal, S. R. Hart, N. Shimizu, E. H. Hauri and G. D. Layne, *Science*, 1998,  
54 529 282, 1481-1484.  
55 530 7. A.E. Saal, S.R. Hart, N. Shimizu, E.H. Hauri, G.D. Layne and J.M. Eiler, *Earth*

- 1  
2  
3  
4 531 *Planet. Sci. Lett.*, 2005, 240, 605-620.
- 5 532 8. J. MacLennan, *Cosmochim. Acta.*, 2008, 72, 4159-4176.
- 6  
7 533 9. H. Yurimoto, T. Kogiso, K. Abe, H. G. Barszczus, A. Utsunomiya and S.  
8  
9 534 Maruyama, *Earth Planet. Int.*, 2004, 146, 231-242.
- 10 535 10. B. Paul, J. D. Wood and J. Hergt, *Anal. Atom. Spect.*, 2005, 20, 1350-1357.
- 11 536 11. A. J. R. Kent, *J. Anal. Atom. Spect.*, 2008, 23, 968-975.
- 12 537 12. A. K. Souders and P. J. Sylvester, *J. Anal. Atom. Spect.*, 2008, 23, 535-543.
- 13  
14 538 13. B. Paul, J. D. Woodhead, J. Hergt, L. Danyushevsky, T. Kunihiro and E.  
15  
16 539 Nakamura, *Chem. Geol.*, 2011, 298, 210-223.
- 17 540 14. S. M. Eggins, L. P. J. Kinsley, and J. M. G. Shelley, *Appl. Surf. Sci.*, 1998,  
18  
19 541 127-129, 278-286.
- 20 542 15. S. E. Jackson, N. J. Pearson, W. L. Griffin, and E. A. Belousova, *Chem. Geol.*,  
21  
22 543 2004, 211, 47-69.
- 23 544 16. M. Tiepolo, C. Bouman, R. Vannuccl and J. Schwieters, *Appl. Geochem.*, 2006,  
24  
25 545 21, 788-801.
- 26 546 17. GeoReM, Max-Planck-Institute data base for geological and environmental  
27  
28 547 reference materials, <http://georem.mpch-mainz.gwdg.de/>.
- 29 548 18. GSJ geochemical reference samples database, <https://gbank.gsj.jp/geostandards/>.
- 30 549 19. S. A. Wilson, Preliminary Certificate of Analysis: Nephelinite, Knippa, Texas,  
31  
32 550 NKT-1G. US Geological Survey Open-File Report. 2006, 2006-xx.
- 33 551 20. P. J. Potts, M. Thompson and S. Wilson, *Geostand. Newsl.*, 2002, 26, 197-235.
- 34 552 21. J. D. Woodhead and J. M. Hergt, *Geostand. Newslett.*, 2001, 25, 261-266.
- 35 553 22. K. A. Matthews, M. T. Murrell, S. J. Goldstein, A. J. Nunn and D. E. Norman,  
36  
37 554 *Geostand. Geoanal. Res.*, 2011, 35, 227-234.
- 38 555 23. Z. Y. Ren, S. Ingle, E. Takahashi, N. Hirano and T. Hirata, *Nature*, 2005, 436,  
39  
40 556 837-840.
- 41 557 24. A. K. Souders and P. J. Sylvester, Use of multiple channeltron ion counters for  
42  
43 558 LA-MC-ICP-MS analysis of common lead isotopes in silicate glasses, in  
44  
45 559 Laser-Ablation-ICPMS in the Earth Science: Principles and Applications, ed. P.  
46  
47 560 Sylvester, Mineral. Assoc. Can. Short Course Series, 2008, 40, 265-281.
- 48 561 25. K. J. R. Rosman and P. D. P. Taylor. *Pure Appl. Chem.*, 1998, 70, 217-235.
- 49 562 26. I. V. Chernyshev, A. V. Chugaev and K. N. Shatagin, *Geochem. Int.*, 2007, 45,  
50  
51 563 1065-1076.
- 52 564 27. H. K. Cooper, M. J. M. Duke, A. Simonetti and G. C. Chen, *J. Archaeol. Sci.*,

- 1  
2  
3  
4 565 2008, 35, 1732-1747.
- 5 566 28. Karla Newman, Philip A. Freedman, Jamie Williams, Nick S. Belshaw and Alex  
6  
7 567 N. Halliday. *J. Anal. Atom. Spect.*, 2009, 24, 6, 701-848.
- 8  
9 568 29. Z. C. Hu, Y. S. Liu, S. Gao, W. G. Liu, W. Zhang, X. R. Tong, L. Lin, K. Q. Zong,  
10  
11 569 M. Li, H. H. Chen, L. Zhou and L. Yang, *J. Anal. Atom. Spect.*, 2012, 27,  
12  
13 570 1391-1399.
- 14 571 30. P. J. Sylvester, M. Ghaderi, *Chem. Geol.*, 1997, 141, 49-65.
- 15  
16 572 31. J. Košler, H. Fonneland, P. Sylvester, M. Tubrett, and R. B. Pedersen, *Chem.*  
17  
18 573 *Geol.*, 2002, 182, 605-618.
- 19 574 32. S. E. Jackson, N. J. Pearson, W. L. Griffin and E. A. Belousova, *Chem. Geol.*,  
20  
21 575 2004, 211, 47-67.
- 22  
23 576 33. D. L. Tollstrup, L. W. Xie, J. B. Wimpenny, E. Chin, C. T. Lee and Q. Z. Yin,  
24  
25 577 *Geochem. Geophys. Geosyst.*, 2012, 13, DOI:10.1029/2011GC004027.
- 26 578 34. M. Elburg, P. Vroon, B. V. D. Wagt and A. Tchalikian, *Chem. Geol.*, 2005, 223,  
27  
28 579 196-207.
- 29  
30 580 35. D. Weis, B. Kieffer, C. Maerschalk, W. Pretorius and J. Barling, *Geochem.*  
31  
32 581 *Geophys. Geosyst.*, 2005, 6, DOI: 10.1029/2004GC000852.
- 33 582 36. J. Kimura, T. W. Sisson, N. Nakano, M. L. Coombs and P. W. Lipman, *J. Volcanol.*  
34  
35 583 *Geotherm. Res.*, 2006, 151, 51-72.
- 36  
37 584

585

586

587

**Table 1** The chemical compositions of the standard glasses used in this study <sup>a b</sup>

|         | Provider | SiO <sub>2</sub> | TiO <sub>2</sub> | Al <sub>2</sub> O <sub>3</sub> | FeO <sub>t</sub> | MgO   | CaO   | Na <sub>2</sub> O | K <sub>2</sub> O | Pb    | <sup>208</sup> Pb/ <sup>206</sup> Pb | <sup>207</sup> Pb/ <sup>206</sup> Pb | <sup>208</sup> Pb/ <sup>204</sup> Pb | <sup>207</sup> Pb/ <sup>204</sup> Pb | <sup>206</sup> Pb/ <sup>204</sup> Pb |
|---------|----------|------------------|------------------|--------------------------------|------------------|-------|-------|-------------------|------------------|-------|--------------------------------------|--------------------------------------|--------------------------------------|--------------------------------------|--------------------------------------|
| JB-1    | GSJ      | 53.15            | 1.32             | 14.53                          | 8.09             | 7.71  | 9.25  | 2.77              | 1.43             | 3.5   | 2.1058                               | 0.8480                               | 38.644                               | 15.561                               | 18.351                               |
| JB-2    | GSJ      | 53.25            | 1.19             | 14.64                          | 10.28            | 4.62  | 9.82  | 2.04              | 0.42             | <1    | 2.0868                               | 0.8484                               | 38.278                               | 15.562                               | 18.343                               |
| NIST612 | NIST     | 72.1             | 0.01             | 2.03                           | 0.01             | 0.01  | 11.9  | 13.7              | 0.02             | 38.57 | 2.1645                               | 0.9073                               | 37.000                               | 15.510                               | 17.094                               |
| NIST614 | NIST     | 72.1             | 0.001            | 2.04                           | 0.002            | 0.01  | 11.9  | 13.7              | 0.01             | 2.32  | 2.1013                               | 0.8710                               | 37.4723                              | 15.533                               | 17.83                                |
| TB-1G   | USGS     | 53.7             | 0.85             | 17.05                          | 8.387            | 3.6   | 7.04  | 3.36              | 4.5              | 16    | 2.1063                               | 0.8482                               | 38.6153                              | 15.551                               | 18.33                                |
| NKT-1G  | USGS     | 38.68            | 3.95             | 10.2                           | 12.00            | 14.33 | 13.21 | 3.48              | 1.28             | 3.1   | 1.9992                               | 0.7955                               | 39.215                               | 15.604                               | 19.615                               |
| BHVO-2G | USGS     | 49.8             | 2.79             | 13.6                           | 11.3             | 7.23  | 11.4  | 2.4               | 0.51             | 1.7   | 2.0524                               | 0.8345                               | 38.211                               | 15.536                               | 18.617                               |

<sup>a</sup> The major and trace elements compositions of NIST 612, NIST 614, JB-1 and BHVO-2G are from reference 17. For TB-1G and NKT-1G are from reference 20 and reference 19. For JB-2 are from reference 18. Preferred reference lead ratio values for NIST614 are from reference 36, for NKT-1G and TB-1G are from reference 34, for JB-2 and BHVO-2G are from reference 35 and for JB-1 are from reference 36.

<sup>b</sup> The oxides are in wt% and the lead is in ppm.

588 **Table 2** Laser ablation and LA-MC-ICPMS instrumentation parameters

| <b>MC-ICP-MS</b>             |                                                                       |
|------------------------------|-----------------------------------------------------------------------|
| Instrument                   | Neptune Plus                                                          |
| RF power                     | 1250W (optimized daily)                                               |
| Auxiliary gas (Ar)           | 0.98L min <sup>-1</sup> (optimized daily)                             |
| Sample gas(Ar)               | 0.92L min <sup>-1</sup> (optimized daily)                             |
| Cooling gas(Ar)              | 16.00L min <sup>-1</sup>                                              |
| Measurement mode             | Static                                                                |
| Interface cones              | Ni standard cones<br>Jet sample cone + X Skimmer cone                 |
| Acceleration voltage         | 10kV                                                                  |
| Detection system             | Eight ion counters                                                    |
| Integration time             | 1.049 s/0.131 s/0.262 s                                               |
| <b>Laser ablation system</b> |                                                                       |
| Instrument                   | RESOLution M-50                                                       |
| Beam                         | UV 193 (ArF excimer)                                                  |
| Spot size                    | 13-45 μm                                                              |
| Repetition rate              | 3-10 Hz                                                               |
| Energy density               | 8-9 J cm <sup>-2</sup> /4 J cm <sup>-2</sup> / 2.3 J cm <sup>-2</sup> |
| Attenuation                  | Not used/ 25%/ 50%                                                    |
| Ablation time                | 50 s/30 s                                                             |
| Blank time                   | 40 s/30 s                                                             |
| He gas to cell               | 800 mL min <sup>-1</sup>                                              |
| N <sub>2</sub> gas to cell   | 2 ml min <sup>-1</sup>                                                |

589

590

591 **Table 3** Neptune Plus collector configuration for Pb isotope analysis

| Collector <sup>a</sup>                                                    | IC5               | IC4                    | IC3               | IC2               | IC1               | C      | IC6               | IC7              | IC8              |
|---------------------------------------------------------------------------|-------------------|------------------------|-------------------|-------------------|-------------------|--------|-------------------|------------------|------------------|
|                                                                           | <sup>202</sup> Hg | <sup>204</sup> (Pb+Hg) | <sup>206</sup> Pb | <sup>207</sup> Pb | <sup>208</sup> Pb | 224.10 | <sup>232</sup> Th | <sup>235</sup> U | <sup>238</sup> U |
| <sup>a</sup> IC1 to IC8 are ion counters and C is the center Faraday cup. |                   |                        |                   |                   |                   |        |                   |                  | 594              |
|                                                                           |                   |                        |                   |                   |                   |        |                   |                  | 595              |

596

597

598

**Table 4** Accuracy and precision of lead isotope ratios for samples measured in this study with different laser ablation parameters <sup>a</sup>

| Standard cones assemblage | Total Pb                | Spot size | Repetition rate | Energy | Energy attenuator | Integration time | Ablation time |            | <sup>208</sup> Pb/ <sup>206</sup> Pb | <sup>207</sup> Pb/ <sup>206</sup> Pb | <sup>208</sup> Pb/ <sup>204</sup> Pb | <sup>207</sup> Pb/ <sup>204</sup> Pb | <sup>206</sup> Pb/ <sup>204</sup> Pb |
|---------------------------|-------------------------|-----------|-----------------|--------|-------------------|------------------|---------------|------------|--------------------------------------|--------------------------------------|--------------------------------------|--------------------------------------|--------------------------------------|
| NIST614                   | 2.32 µg g <sup>-1</sup> | 32µm      | 10Hz            | 100mJ  | Not used          | 1.049s           | 50s           | 2RSD n=111 | 0.29%                                | 0.41%                                | 0.98%                                | 0.97%                                | 0.93%                                |
|                           |                         |           |                 |        |                   |                  |               | Accuracy   | 0.06%                                | -0.01%                               | -0.35%                               | -0.41%                               | -0.41%                               |
| NKT-1G                    | 3.01 µg g <sup>-1</sup> | 32µm      | 10Hz            | 80mJ   | 50%               | 1.049s           | 50s           | 2RSD n=20  | 0.42%                                | 0.44%                                | 1.58%                                | 1.62%                                | 1.72%                                |
|                           |                         |           |                 |        |                   |                  |               | Accuracy   | 0.03%                                | -0.13%                               | -0.48%                               | -0.62%                               | -0.54%                               |
| TB-1G                     | 16 µg g <sup>-1</sup>   | 23µm      | 3Hz             | 80mJ   | 50%               | 0.262s           | 30s           | 2RSD n=18  | 0.39%                                | 0.36%                                | 1.64%                                | 1.51%                                | 1.64%                                |
|                           |                         |           |                 |        |                   |                  |               | Accuracy   | 0.20%                                | 0.06%                                | -0.26%                               | -0.41%                               | -0.41%                               |
| NIST614                   | 2.32 µg g <sup>-1</sup> | 23µm      | 3Hz             | 80mJ   | 50%               | 0.131s           | 30s           | 2RSD n=110 | 0.64%                                | 0.79%                                | 4.05%                                | 4.25%                                | 4.17%                                |
|                           |                         |           |                 |        |                   |                  |               | Accuracy   | 0.25%                                | 0.03%                                | 0.51%                                | 0.36%                                | 0.36%                                |
| Jet+X cones assemblage    | Total Pb                | Spot size | Repetition rate | Energy | Energy attenuator | Integration time | Ablation time |            | <sup>208</sup> Pb/ <sup>206</sup> Pb | <sup>207</sup> Pb/ <sup>206</sup> Pb | <sup>208</sup> Pb/ <sup>204</sup> Pb | <sup>207</sup> Pb/ <sup>204</sup> Pb | <sup>206</sup> Pb/ <sup>204</sup> Pb |
| BHVO-2G                   | 1.7 µg g <sup>-1</sup>  | 23µm      | 3Hz             | 80mJ   | 50%               | 0.262s           | 30s           | 2RSD n=20  | 0.60%                                | 0.50%                                | 5.50%                                | 5.30%                                | 5.20%                                |
|                           |                         |           |                 |        |                   |                  |               | Accuracy   | 0.03%                                | -0.05%                               | 1.00%                                | 0.87%                                | 1.02%                                |
| NKT-1G                    | 3.01 µg g <sup>-1</sup> | 23µm      | 3Hz             | 80mJ   | 50%               | 0.262s           | 30s           | 2RSD n=16  | 0.39%                                | 0.35%                                | 3.04%                                | 3.13%                                | 3.13%                                |
|                           |                         |           |                 |        |                   |                  |               | Accuracy   | -0.17%                               | 0.02%                                | -0.77%                               | -0.60%                               | -0.70%                               |
| TB-1G                     | 16 µg g <sup>-1</sup>   | 24µm      | 3Hz             | 80mJ   | 25%               | 0.262s           | 30s           | 2RSD n=18  | 0.19%                                | 0.16%                                | 1.04%                                | 0.88%                                | 0.81%                                |
|                           |                         |           |                 |        |                   |                  |               | Accuracy   | -0.13%                               | -0.12%                               | -0.41%                               | -0.27%                               | -0.22%                               |

<sup>a</sup> Preferred reference values for NIST614 are from reference 21, for NKT-1G and TB-1G are from reference 34, for BHVO-2G are from reference 35 and for JB-1 are from reference 36.

Table 5 Summary of the previous studies

| Authors                             |                           | total Pb                  | system   | detector   |                      | Repetition rate | Spot size           | ablation time |          | $^{208}\text{Pb}/^{206}\text{Pb}$ | $^{207}\text{Pb}/^{206}\text{Pb}$ | $^{208}\text{Pb}/^{204}\text{Pb}$ | $^{207}\text{Pb}/^{204}\text{Pb}$ | $^{206}\text{Pb}/^{204}\text{Pb}$ |
|-------------------------------------|---------------------------|---------------------------|----------|------------|----------------------|-----------------|---------------------|---------------|----------|-----------------------------------|-----------------------------------|-----------------------------------|-----------------------------------|-----------------------------------|
| Saal et al. <sup>7</sup>            | Loihi glass               | 3 $\mu\text{g g}^{-1}$    | SIMS     |            |                      |                 | 20-30 $\mu\text{m}$ |               | 2RSD     | 0.66%                             | 0.50%                             |                                   |                                   |                                   |
| Paul et al. <sup>10</sup>           | BCR-2G                    | 10 $\mu\text{g g}^{-1}$   | MC-ICPMS | Faraday-IC | 5J $\text{cm}^{-2}$  | 6Hz             | 93 $\mu\text{m}$    | 60s           | 2RSD     | 0.11%                             | 0.22%                             | 0.38%                             | 0.42%                             | 0.40%                             |
|                                     |                           |                           |          |            |                      |                 |                     |               | Accuracy | 0.15%                             | 0.12%                             | 0.07%                             | 0.21%                             | 0.21%                             |
|                                     | MPI-ATHO                  | 6 $\mu\text{g g}^{-1}$    |          |            | 5J $\text{cm}^{-2}$  | 6Hz             | 93 $\mu\text{m}$    | 60s           | 2RSD     | 0.30%                             | 0.47%                             | 0.48%                             | 0.59%                             | 0.60%                             |
|                                     |                           |                           |          |            |                      |                 |                     |               | Accuracy | 0.00%                             | 0.24%                             | 0.04%                             | 0.30%                             | 0.30%                             |
|                                     | MPI-KL-2G                 | 2 $\mu\text{g g}^{-1}$    |          |            | 5J $\text{cm}^{-2}$  | 6Hz             | 93 $\mu\text{m}$    | 60s           | 2RSD     | 0.70%                             | 1.06%                             | 1.47%                             | 1.76%                             | 1.43%                             |
|                                     |                           |                           |          |            |                      |                 |                     |               | Accuracy | -0.05%                            | 0.61%                             | -0.24%                            | 0.88%                             | 0.72%                             |
| Kent <sup>11</sup>                  | BCR-2G                    | 10 $\mu\text{g g}^{-1}$   | MC-ICPMS | Faraday-IC | 12J $\text{cm}^{-2}$ |                 |                     |               | 2RSD     | 0.14%                             | 0.37%                             | 0.41%                             | 0.30%                             | 0.61%                             |
|                                     |                           |                           |          |            |                      |                 |                     |               | Accuracy | 0.10%                             | 0.12%                             | -0.05%                            | 0.12%                             | -0.05%                            |
|                                     | NIST614                   | 2.31 $\mu\text{g g}^{-1}$ |          |            |                      |                 |                     |               | 2RSD     | 0.23%                             | 0.37%                             | 0.54%                             | 0.52%                             | 0.56%                             |
|                                     |                           |                           |          |            |                      |                 |                     |               | Accuracy | -0.14%                            | 0.46%                             | -0.29%                            | 0.44%                             | -0.12%                            |
| Souders and Sylvester <sup>12</sup> | MPI-T1-G                  | 11.6 $\mu\text{g g}^{-1}$ | MC-ICPMS | IC         | 5J $\text{cm}^{-2}$  | 10Hz            | 40 $\mu\text{m}$    | 50s           | 2RSD     | 0.36%                             | 0.22%                             | 0.83%                             | 0.78%                             | 0.70%                             |
|                                     |                           |                           |          |            |                      |                 |                     |               | Accuracy | 0.02%                             | -0.07%                            | 0.03%                             | -0.04%                            | 0.04%                             |
|                                     | MPI-ATHO-G                | 5.67 $\mu\text{g g}^{-1}$ |          |            | 5J $\text{cm}^{-2}$  | 10Hz            | 40 $\mu\text{m}$    | 50s           | 2RSD     | 0.31%                             | 0.31%                             | 1.91%                             | 1.98%                             | 2.10%                             |
|                                     |                           |                           |          |            |                      |                 |                     |               | Accuracy | 0.26%                             | -0.09%                            | -0.14%                            | -0.23%                            | -0.09%                            |
|                                     | MPI-KL2-G                 | 2.07 $\mu\text{g g}^{-1}$ |          |            | 5J $\text{cm}^{-2}$  | 10Hz            | 69 $\mu\text{m}$    | 50s           | 2RSD     | 0.40%                             | 0.34%                             | 2.59%                             | 2.51%                             | 2.82%                             |
|                                     |                           |                           |          |            |                      |                 |                     |               | Accuracy | 0.16%                             | -0.01%                            | 0.15%                             | 0.01%                             | 0.12%                             |
| MPI-ML3B-G                          | 1.38 $\mu\text{g g}^{-1}$ |                           |          |            | 5J $\text{cm}^{-2}$  | 10Hz            | 69 $\mu\text{m}$    | 50s           | 2RSD     | 0.53%                             | 0.34%                             | 2.71%                             | 2.73%                             | 2.73%                             |
|                                     |                           |                           |          |            |                      |                 |                     |               | Accuracy | -0.30%                            | -0.45%                            | -1.59%                            | -1.49%                            | -1.07%                            |

**Table 6** Lead isotope ratios for melt inclusion YX-11-1(3)-8 in this study <sup>a</sup>

|                                                                                                                                                             |              | <sup>208</sup> Pb/ <sup>206</sup> Pb | 1SE    | <sup>207</sup> Pb/ <sup>206</sup> Pb | 1SE    | <sup>208</sup> Pb/ <sup>204</sup> Pb | 1SE    | <sup>207</sup> Pb/ <sup>204</sup> Pb | 1SE    | <sup>206</sup> Pb/ <sup>204</sup> Pb | 1SE    |
|-------------------------------------------------------------------------------------------------------------------------------------------------------------|--------------|--------------------------------------|--------|--------------------------------------|--------|--------------------------------------|--------|--------------------------------------|--------|--------------------------------------|--------|
| BHVO-2G <sup>b</sup>                                                                                                                                        | Mean (n=116) | 2.0557                               |        | 0.8336                               |        | 38.5594                              |        | 15.6361                              |        | 18.7568                              | 624    |
|                                                                                                                                                             | 2RSD         | 0.27%                                |        | 0.30%                                |        | 1.45%                                |        | 1.53%                                |        | 1.45%                                | 625    |
|                                                                                                                                                             | Accuracy     | 0.16%                                |        | -0.10%                               |        | 0.91%                                |        | 0.65%                                |        | 0.75%                                | 625    |
| YX-11-1(3)-8a                                                                                                                                               |              | 2.0888                               | 0.0015 | 0.8375                               | 0.0008 | 38.9711                              | 0.1537 | 15.6565                              | 0.0640 | 18.6771                              | 0.0626 |
| YX-11-1(3)-8b                                                                                                                                               |              | 2.0882                               | 0.0013 | 0.8367                               | 0.0006 | 39.1371                              | 0.1384 | 15.6876                              | 0.0547 | 18.7607                              | 0.0641 |
| YX-11-1(3)-8c                                                                                                                                               |              | 2.0897                               | 0.0016 | 0.8379                               | 0.0006 | 38.6568                              | 0.1390 | 15.5206                              | 0.0547 | 18.5324                              | 0.0671 |
|                                                                                                                                                             | 2RSD         | 0.07%                                |        | 0.15%                                |        | 1.25%                                |        | 1.14%                                |        | 1.24%                                | 628    |
| <sup>a</sup> The laser parameters are 45μm spot, 3Hz repetition rate and 80 mJ energy with a 25% energy attenuator (2.3 J cm <sup>-2</sup> energy density). |              |                                      |        |                                      |        |                                      |        |                                      |        |                                      | 629    |
| <sup>b</sup> Preferred reference values for BHVO-2G are from reference 35.                                                                                  |              |                                      |        |                                      |        |                                      |        |                                      |        |                                      |        |



630

**Figure captions**

**Fig. 1** Statistics of olivine-hosted melt inclusion sizes. These olivine-hosted melt inclusions are from basalts in the Hannuoba (343), Hainan (301), Emeishan LIP (296) and Hawaii (508) volcanoes. 42% of the melt inclusions have diameters larger than 40  $\mu\text{m}$ ; only 9.5% melt inclusions are larger than 80  $\mu\text{m}$ .

636

**Fig. 2** Relationship between internal precision of single spot analysis and ablation time for NKT-1G. As laser ablation time increases, the internal precision improves. When the ablation time of a single laser spot is longer than 30 s, the precisions of Pb isotope ratios stabilize. The laser parameters are 45  $\mu\text{m}$  spot, 3Hz repetition rate and 80 mJ energy with a 25% energy attenuator ( $\sim 2.3 \text{ J cm}^{-2}$  energy density). A Jet sample cone and X skimmer cone were used. Under this laser ablation condition the  $^{208}\text{Pb}$  intensity of NKT-1G is about 260000 cps.

644

**Fig. 3** Pb isotope analysis of NIST 614 with 32  $\mu\text{m}$  laser spot size, 10 Hz repetition rate and 9  $\text{J cm}^{-2}$  energy density. The preferred values are from reference 21. The error bars correspond to 1 standard error (1SE).

648

649

**Fig. 4** Pb isotope analysis of NIST 614 using 23  $\mu\text{m}$  laser spot size, 3 Hz repetition rate and 80 mJ energy with a 50% energy attenuator ( $4 \text{ J cm}^{-2}$  energy density). The preferred values are from reference 21. The error bars correspond to 1 standard error (1SE).

654

655

**Fig. 5** Variations of Pb isotope ratios during a single spot analysis of NIST 614 using (a) the standard cones assemblage and (b) the Jet sample cone and X skimmer cone assemblage. The same laser parameters (spot size: 23  $\mu\text{m}$ ; repetition rate: 3 Hz; energy: 80; energy density:  $4 \text{ J cm}^{-2}$ ) were used in both cases. In the former case, the signal intensity for  $^{208}\text{Pb}$  is about 22000 cps, while in the later case, it is about 65000 cps.

662

663

664 **Fig. 6** a, b Comparison of the external precision of  $^{208}\text{Pb}/^{206}\text{Pb}$  and  $^{208}\text{Pb}/^{204}\text{Pb}$  using  
665 (a) the standard cones assemblage and (b) the Jet and X skimmer cones assemblage.  
666 Using the Jet and X cones, under the same laser ablation condition, the precisions for  
667 almost all the samples are improved at least by a factor of two compared to using the  
668 standard cones. c, d Relationship between external precision and signal intensity for  
669  $^{208}\text{Pb}/^{206}\text{Pb}$  and  $^{208}\text{Pb}/^{204}\text{Pb}$ . Filled symbols measured with the Jet and X cones, open  
670 symbols measured with the standard cones. The numbers in parentheses show laser  
671 spot sizes. The curves are fitted from the experimental data. For the samples in  
672 Souders and Sylvester<sup>12</sup> (gray filled circles), we assumed that the signal intensity was  
673 proportional to laser ablation area. Note that at  $^{208}\text{Pb}$  signal intensity  $> 200000$  cps,  
674 external precisions of ratios involving  $^{204}\text{Pb}$  are better than 1.3% (2RSD) and  
675 precisions of  $^{208}\text{Pb}/^{206}\text{Pb}$  and  $^{207}\text{Pb}/^{206}\text{Pb}$  are better than 0.23% (2RSD). All the data in  
676 a, b, c and d were measured using a 3 Hz repetition rate and 80 mJ energy with a 25%  
677 energy attenuator ( $\sim 2.3 \text{ J cm}^{-2}$  energy density). Only the laser spot sizes varied  
678 between the different analyses.

679

680

681 **Fig. 7** Pb isotope analysis of BHVO-2G with a 45  $\mu\text{m}$  laser spot size, 3Hz repetition  
682 rate and and 80 mJ energy with a 25% energy attenuator ( $\sim 2.3 \text{ J cm}^{-2}$  energy density).  
683 The white open circles showing the preferred values fall within the fields defined by  
684 the *in situ* analyses. The error bars correspond to 1 standard error (1SE).

685

686

687 **Fig. 8** Representative time-resolved data acquired during laser ablation analysis of  
688 NKT-1G. A linear correlation method was used to correct for downhole fractionation.

689

690

691 **Fig. 9** The Pb isotope ratios for melt inclusions from the Emeishan flood basalt. The  
692 small circles are age-uncorrected Pb isotope ratios and the diamonds are age-corrected.  
693 The error bars correspond to 2 standard error. The Pb isotope data for the Emeishan  
694 melt inclusions are from Ren et al. unpublished data.

695

696

Fig. 1

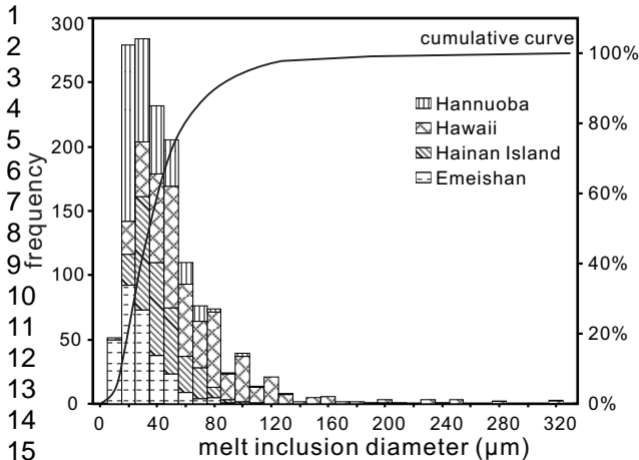


Fig. 2

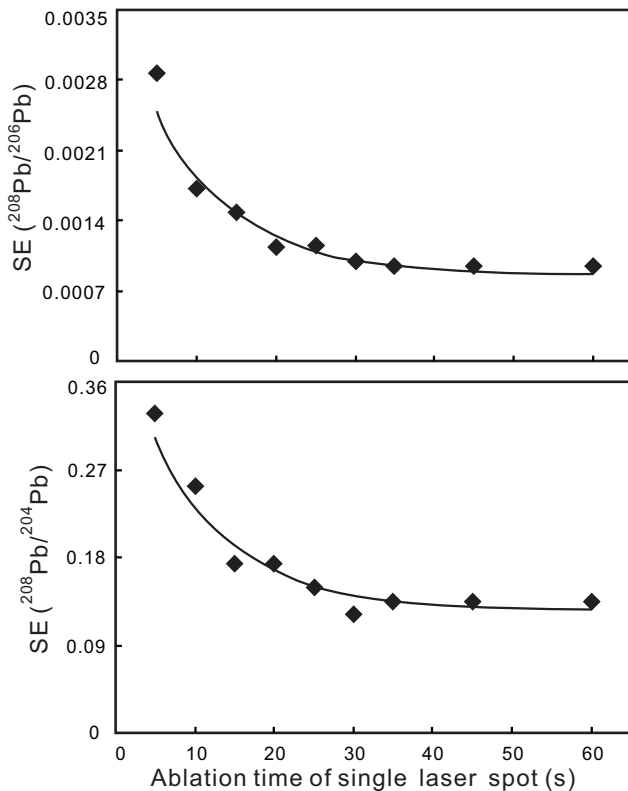


Fig. 3

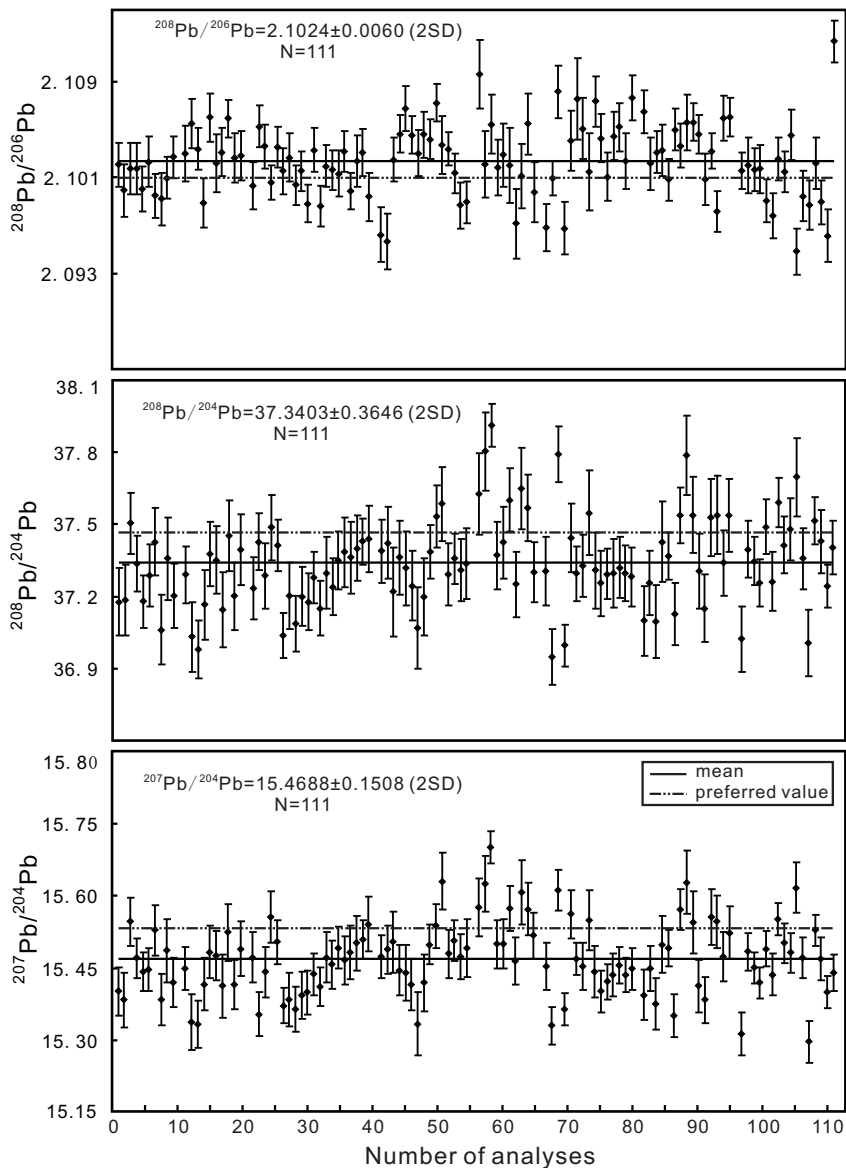


Fig. 4

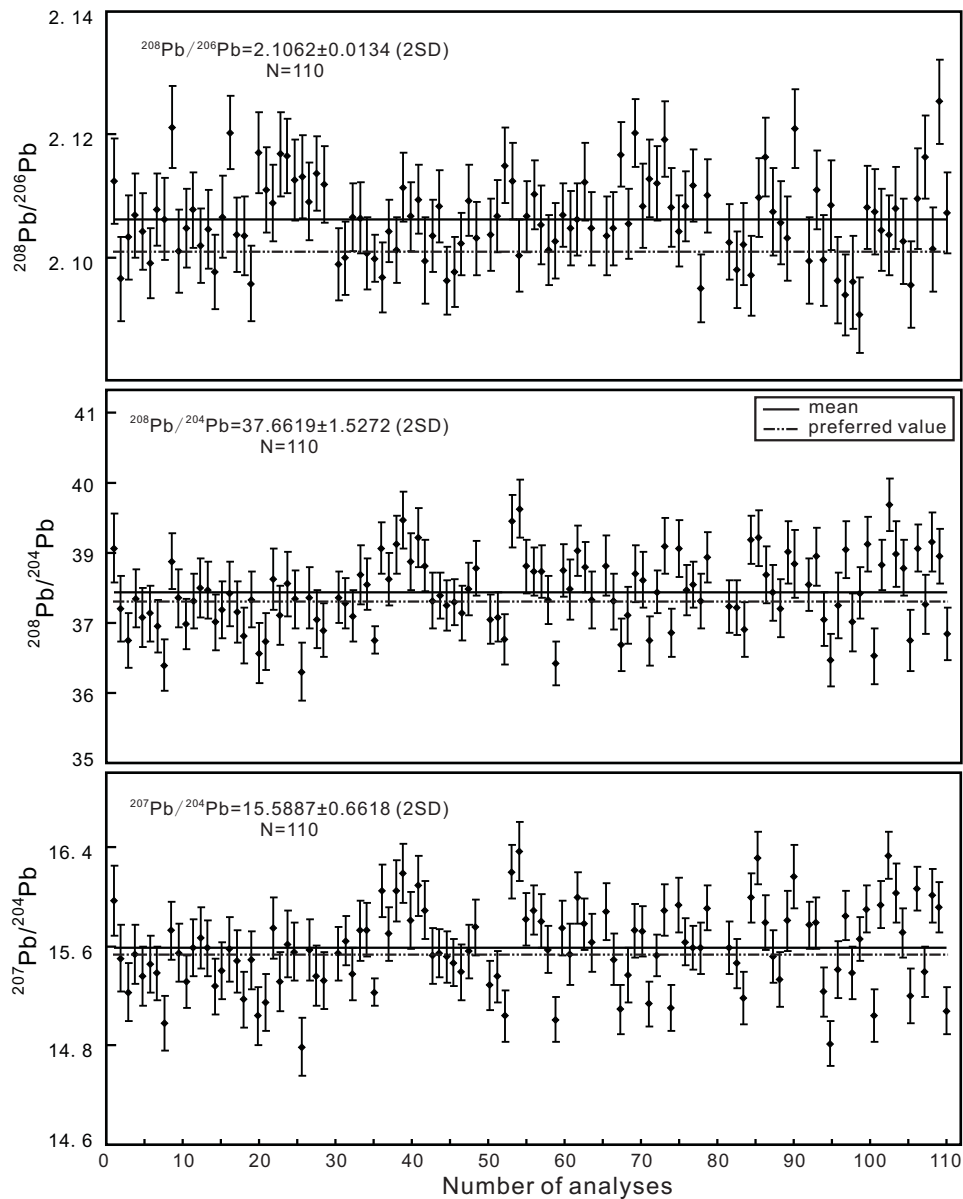


Fig. 5

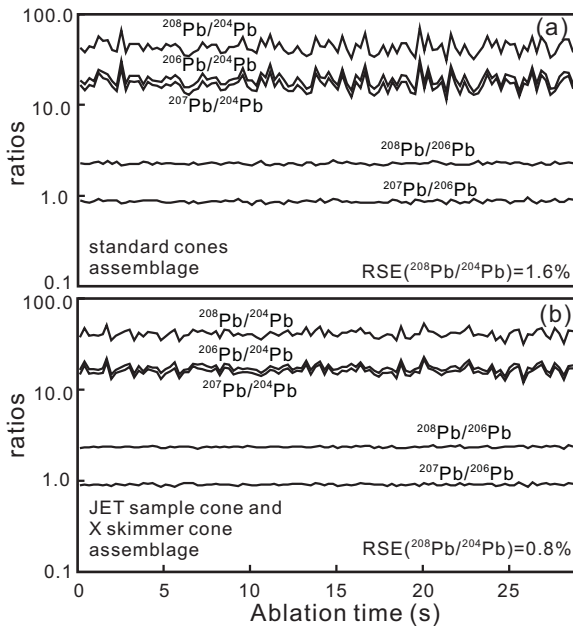


Fig. 6

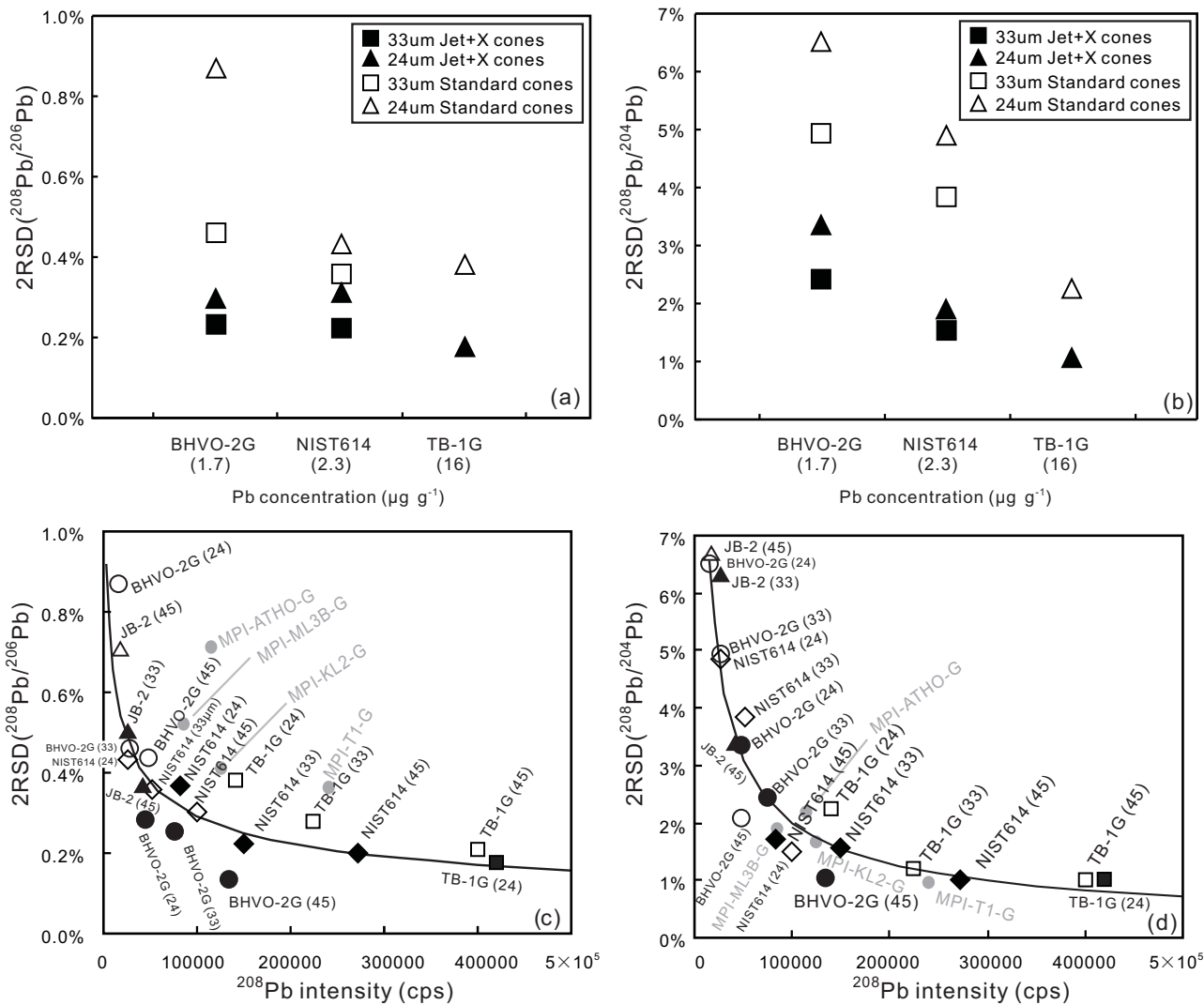




Fig. 7

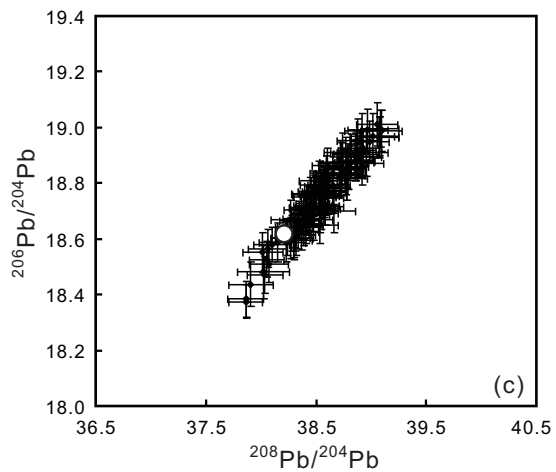
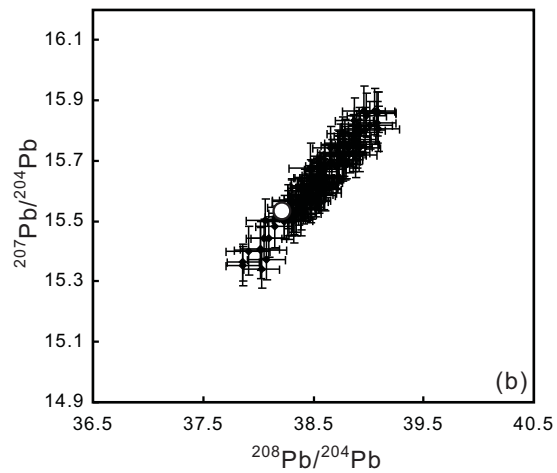
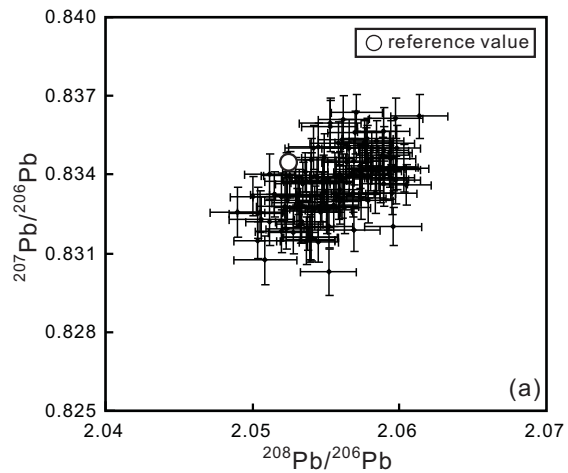


Fig. 8

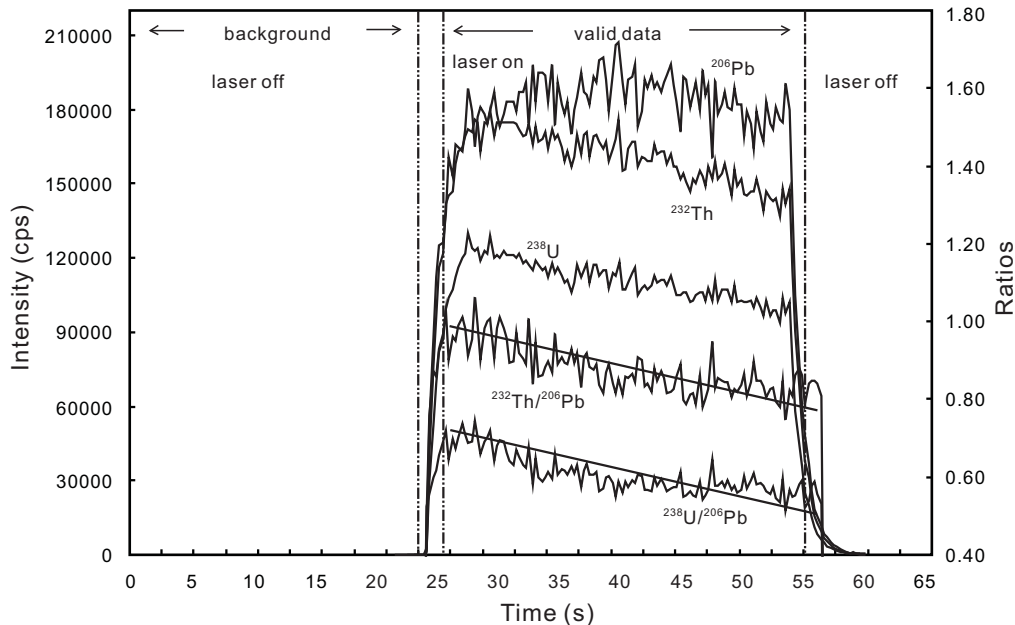


Fig. 9

